Critical role for mesoscale eddy diffusion in supplying oxygen to hypoxic ocean waters

Anand Gnanadesikan,[1] Daniele Bianchi,[2] and Marie-Aude Pradal[1]

Received 19 August 2013; revised 16 September 2013; accepted 26 September 2013.

[1] Estimates of the oceanic lateral eddy diffusion coefficient A_{redi} vary by more than an order of magnitude, ranging from less than a few hundred m^2/s to thousands of m^2/s. This uncertainty has first-order implications for the intensity of oceanic hypoxia, which is poorly simulated by the current generation of Earth System Models. Using satellite-based estimate of oxygen consumption in hypoxic waters to estimate the required diffusion coefficient for these waters gives a value of order 1000 m^2/s. Varying A_{redi} across a suite of Earth System Models yields a broadly consistent result given a thermocline diapycnal diffusion coefficient of 1×10^{-5} m^2/s. **Citation:** Gnanadesikan, A., D. Bianchi, and M.-A. Pradal (2013), Critical role for mesoscale eddy diffusion in supplying oxygen to hypoxic ocean waters, *Geophys. Res. Lett.*, *40*, doi:10.1002/grl.50998.

1. Introduction

[2] Hypoxic waters (here defined as $0\ \mu M < O_2 < 88\ \mu M$), in which fish and higher organisms become physiologically stressed, can be found at some depth in water column over ~1/3 of the ocean area (Figure 1a), account for about 10% of the volume of the oceans [*Bianchi et al*., 2012] and are expected to increase in volume as a result of climate change [*Stramma et al*., 2010]. The intensity of oceanic hypoxia plays an important role in global biogeochemical cycling. Waters where oxygen concentrations drop below 20 μM (defined here as suboxic, Figure 1b) show evidence of denitrification, which removes reactive nitrogen from ocean ecosystems and in isolation represents a source of carbon dioxide to the atmosphere. [*Gruber and Sarmiento*, 1997]. The volume of waters with oxygen concentrations less than 20 μM is around 16 Mkm^3 with about 1/3 of these waters dropping below 10 μM (solid black line, Figures 1c, 1d).

[3] The Earth System Models used for projecting future climate change have significant difficulty in predicting the volume census of these low-oxygen waters, as illustrated by the subset of published models shown in Figure 1c (for more detail, see the distribution of oxygen at intermediate depths and the distribution of hypoxic and suboxic waters in Figures S1–S3 of the supporting information). The Max-Planck Institute ESM-LR model [*Jungclaus et al*., 2010] is biased high by a factor of 4.89 over the range of 10–100 uM with 15 times too much water at concentrations below 10 μm. This is despite this model having one of the more realistic spatial distributions of oxygen (Figure S1). The HadGEM model [*Jones et al*., 2010] is biased too low by a factor 3. The IPSL-CM5A-LR model [*Seferian et al*., 2012], while roughly matching observations at values below 10 μM, significantly overpredicts the amount of hypoxic water, as the entire deep North Pacific drops below concentrations of 88 μM (Figure S2, S3), and the GFDL ESM2.1 model [*Gnanadesikan et al*., 2012] generally overpredicts the amount of suboxia—though it does come close to matching observations at higher oxygen levels. While models simulate the rough location of suboxic waters along the eastern ocean edges, they generally miss many of the details of their structure.

[4] *Gnanadesikan et al*. [2012] demonstrated the important role of lateral diffusion in supplying oxygen to suboxic waters. The lateral diffusion coefficient A_{redi} [*Redi*, 1982] representing the stirring of passive tracers along isopycnal surfaces is very poorly constrained in the tropics. Estimates from baroclinic instability theory [*Visbeck et al*., 1997] give relatively low values of around 100–300 m^2/s. Estimates of lateral diffusivity in midlatitudes based on the release of chlorofluorocarbon tracers [*Ledwell et al*., 1998] give values ranging from 800 m^2/s to 2200 m^2/s and midlatitude float release experiments [e.g., *Ollitraut and Colin de Verdiere*, 2002] give even higher values. However, these latter two estimates suffer from the difficulty of separating dispersion due to mean flows (which may be resolved by coarse models) from dispersion due to unresolved eddies. In this paper, we consider the role of this diffusion coefficient in altering oxygen concentrations in a set of Earth System Models, and estimate it from the distribution of oxygen and satellite-based estimates of oxygen demand. Both methods suggest A_{redi} of order 1000 m^2/s in low latitudes.

2. Methods

2.1. Experimental Design: ESM Sensitivity

[5] The Earth System Model ESM2Mc, which is used for the sensitivity study is described in *Galbraith et al*. [2011]. It consists of a nominally $3° \times 1°$ ocean with 28 vertical levels, nine of which cover the top 100 m, and a 3° atmosphere with 24 levels. The model contains up-to-date representations of planetary boundary layers, tidal

Additional supporting information may be found in the online version of this article.

[1]Department of Earth and Planetary Sciences, John Hopkins University, Baltimore, Maryland, USA.
[2]Earth and Planetary Sciences, McGill University, Montreal, Quebec, Canada.

Corresponding author: A. Gnanadesikan, Department of Earth and Planetary Sciences, John Hopkins University, Olin Hall, 3400 N. Charles St., Baltimore, MD 21218, USA. (gnanades@jhu.edu)

0094-8276/13/10.1002/grl.50998

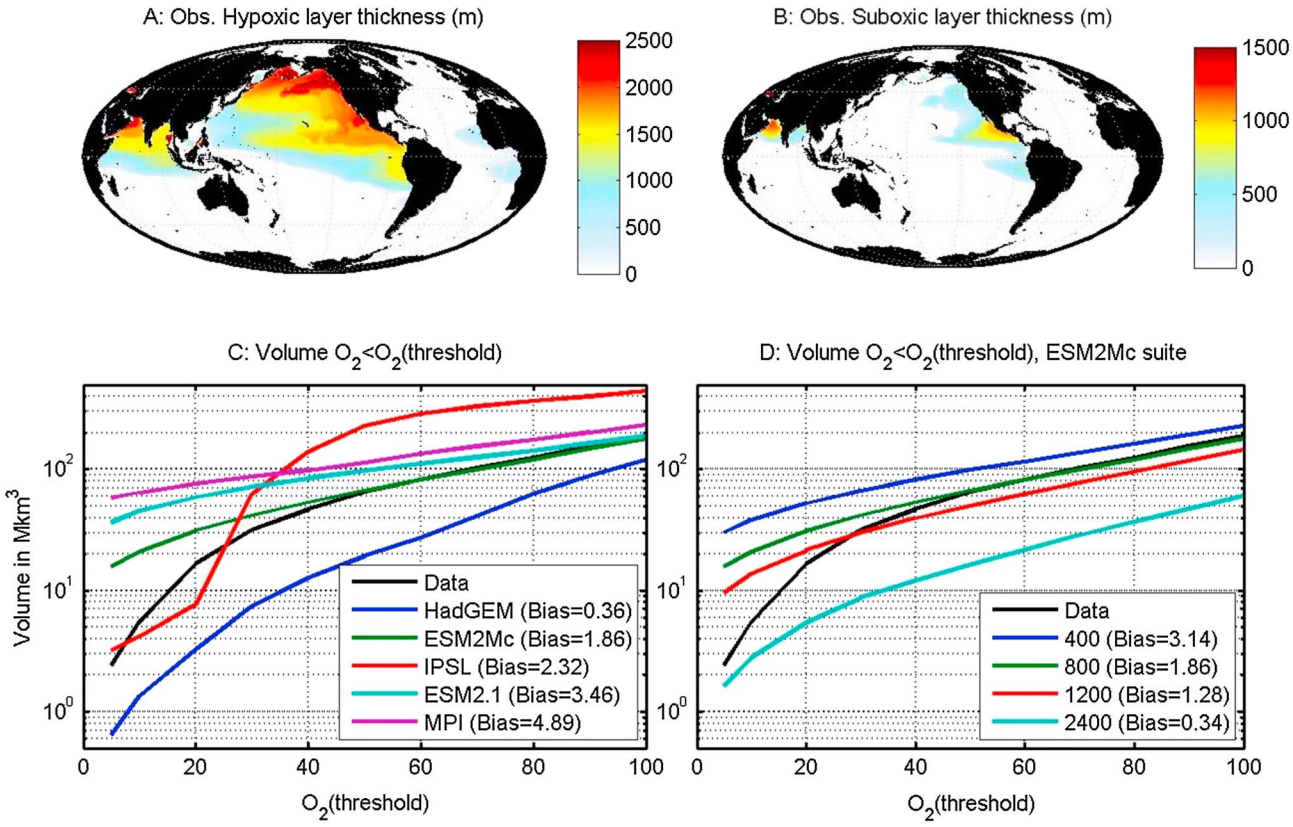

Figure 1. Hypoxia and suboxia in the ocean. (a) Thickness of hypoxic water column ($O_2 < 88$ μM) from *Bianchi et al.* [2012] correction to World Ocean Atlas 2005 data set. (b) Same as Figure 1a but for suboxic column thickness ($O_2 < 20$ μM). (c) Volume of water with O_2 less than some threshold (horizontal axis) in data (thick black line) and five published Earth System Models (colored lines). Biases averaged over the 10 thresholds shown (10–100 μM). (d) Same as Figure 1c but with four versions of ESM2Mc with different lateral diffusion coefficients A_{redi}.

generation of ocean diapycnal mixing, atmospheric gravity wave drag, radiation, and cloud physics identical to the higher-resolution ESM2.1 model. The background diffusion coefficient in the ocean is 1×10^{-5} m^2/s. The control model produces a reasonable climate with global RMS SST (sea surface temperature) errors of around 1.7°C and tropical RMS SST errors around 1.4°C, a North Atlantic Overturning of ~20*Sv*, and an El Niño–Southern Oscillation that is close to observed amplitude. *Galbraith et al.* [2011] provide more details. The formation of deep waters in the North Pacific in the control is too strong, as reflected by the oxygen field (Figure S1) which fails to capture the extension of low oxygen waters into this region.

[6] The biogeochemical component is the Biology, Light, Iron Nutrient, and Gasses (BLING) code [*Galbraith et al.*, 2010]. This code uses the nutrient, light, and temperature produced by the model to compute phytoplankton growth rates. These growth rates are then used to solve for a steady state biomass and associated uptake rates of iron and nutrient. The fraction of nutrient exported as particulate matter depends on the growth rate and temperature, with the export fit to the data set of *Dunne et al.* [2005]. Organic material sinks with a constant velocity of 16 m/day over the top 80 m, with the sinking velocity increasing by 0.05 m/day/m below that depth. The rate of remineralization of organic material depends on the oxygen concentration,

$$\gamma^{POP} = \gamma_0^{POP} \times \frac{[O_2]^2}{k_{O2}^2 + [O_2]^2}, \quad (1)$$

with $k_{O2} = 20$ μM following the TOPAZ model used in ESM2.1., [*Dunne et al.*, 2010].

[7] Results were generated from a control version of the model which had been spun up for 1500 years with a diffusion coefficient of 800 m^2/s. The model was initialized with ocean data from the World Ocean Atlas 2001 and run with constant 1860 radiative conditions. At year 1500, lateral diffusion coefficients were changed to values of 400, 1200, and 2400 m^2/s, and the model was allowed to equilibrate for 500 years. Only 1.5–7.5% of the total change in suboxic volume occur in the final century. Most of the adjustment of suboxic volumes occur within the first 150 years.

2.2. Estimating A_{redi} From Data

[8] Consider the oxygen budget within closed isosurfaces of oxygen. When a time average is taken, long-term advection of oxygen by the mean flow across mean isosurfaces drops to zero, as any mass flux into the enclosed volume must be balanced by a mass flux which leaves the volume at the same concentration of oxygen as the entering flux. This means that the dominant fluxes are associated with some sort of time-varying advection associated with eddy or wave processes, represented by diffusion coefficients. Letting the diffusion coefficient across isopycnal surfaces

Table 1. Oxygen Balance Within Different Isosurfaces of Oxygen[a]

O_2	J_{O2} (mmol/m^3/yr)	Vertical Diffusive Supply, $K_v = 10^{-5}$	Lateral Diffusive Supply	Implied Lateral Diffusion Coefficient
88	0.76	0.10	0.66	1015
50	1.09	0.16	0.93	926
20	1.54	0.17	1.37	934
10	2.00	0.16	1.84	1035

[a]J_{O2} shows satellite-based estimates of oxygen consumption. Vertical diffusive supply computed from observed distribution assuming a diffusion coefficient of 10^{-5} m^2/s. Lateral diffusive supply is the residual of oxygen sink J_{O2} and vertical diffusive supply. Implied lateral diffusion coefficient is value needed to operate on the observed distribution of oxygen to produce the supply in column 4.

be denoted as K_v, taking both A_{redi} and K_v as constants, and assuming that density surfaces in the oxygen minimum zones have slopes $<<1$, we can define the following steady state balance

$$\iiint J_{O2}\mathrm{d}V + \iiint A_{redi}\nabla_s^2 O_2 + K_v\left(\frac{\partial\rho}{\partial z}\right)^2\frac{\partial^2 O_2}{\partial\rho^2}\mathrm{d}V = 0, \quad (2)$$

where J_{O2} are oxygen sinks due to respiration, ∇_s denotes gradients along an isopycnal surface and the integral denotes integration over a volume enclosed by an isosurface (see supporting information for full derivation). The "small slope" approximation allows us to orient the diapycnal mixing largely along the vertical direction, a reasonable assumption outside of the well-oxygenated mixed layer. Rearranging equation (2), we find that

$$A_{redi} = \left(\iiint J_{O2} - K_v\left(\frac{\partial\rho}{\partial z}\right)^2\frac{\partial^2 O_2}{\partial\rho^2}\right)\mathrm{d}V \Big/ \iiint\nabla_s^2 O_2\mathrm{d}V, \quad (3)$$

so that if we know the net oxygen consumption, the spatial distribution of oxygen, and the vertical diffusion coefficient, we can come up with an estimate for the lateral diffusion coefficient.

[9] The sink of oxygen J_{O2} is estimated following *Bianchi et al*. [2012]. The first step uses the export production of *Dunne et al*. [2007]

$$\text{Export Production} = \text{Primary Production} \times Pe_{ratio} \quad (4)$$

where

$$Pe_{ratio} = 0.426 - 0.0081^{\circ}C^{-1} \times T + 0.068 \times \ln(\mathrm{chl}/Z_{eu})$$
$$0.04 < Pe_{ratio} < 0.72 \quad (5)$$

and T is the temperature in °C, chl is the chlorophyll concentration in mg/m^3, Z_{eu} is the euphotic zone depth in m, and primary production is estimated as the mean of three satellite products [*Behrenfeld and Falkowski*, 1997; *Carr*, 2002; *Marra et al*., 2003]. The export production then provides a vertical flux at 75 m. In nonsuboxic waters below 75 m, this flux is assumed to have a profile that satisfies the equation

$$\frac{\partial\Phi}{\partial z} = \frac{b\Phi}{z} \quad (6)$$

where $b = 0.8$ for all z. At very low oxygen ($O_2 < 4.5$ μM), the coefficient b is set to 0.36, capturing the difference between the open ocean and low-oxygen Mexican margin in sediment-trap based flux profiles [*Hartnett and Devol*, 2003]. Oxygen consumption is then estimated from the divergence of the export flux, assuming a stoichiometric ration of 170:106 for oxygenated waters. Unfortunately, the rate of oxygen consumption close to anoxic conditions (when the oxidant for a significant fraction of the organic matter consumed is nitrate) is largely unconstrained. We find that, for equation (3) to give realistic (nonnegative) isopycnal diffusivities close to anoxia, a nonzero oxygen consumption rate is required. Therefore, for $O_2 < 4.5$ μM, we calculate this rate as 60% of the total remineralization rate, noting that values between 40–80% provide values of A_{redi} in the suboxic range that are similar to the values obtained for the rest of the oxygen range. Additionally, given these uncertainties, we exclude from our estimate of A_{redi} values obtained for threshold values of $O_2 < 10$ μM. The resulting rates of oxygen demand (Table 1) are of order 1 mmol/m^3/yr with an approximate variation over a factor of 3 between all hypoxic waters and those with $O_2 < 10$ μM which are located under relatively productive regions.

3. Results

3.1. ESM Results

[10] In the ESM2Mc simulations, changing A_{redi} has a first-order impact on suboxic volume. While the control case with $A_{redi} = 800$ m^2/s (green line, Figures 1c,1d) settles down to a volume of 31 Mkm^3, about twice the observed value, the low-diffusion $A_{redi} = 400$ m^2/s has a volume of 51 Mkm^3 and the high diffusion $A_{redi} = 2400$ m^2/s case has a value of 5.4 Mkm^3, which is too low. The range of diffusion coefficients results in a range of hypoxic volumes at the high end of the curve of 83–227 Mkm^3, with the best match at $A_{redi} = 800$ m^2/s. The changes in diffusion coefficient change the intensity of hypoxia and suboxia, but have relatively little impact on the geographic location (Figures S1–S3).

[11] Interior oxygen concentrations can be divided into a saturation component determined by temperature and salinity and an oxygen utilization associated with the consumption of organic matter. Overly intense hypoxia could then result from

[12] 1. Surface oxygen concentrations being systematically too low due to waters being too warm or insufficiently oxygenated.

[13] 2. The rate of oxygen consumption being systematically too high, either because surface waters are too productive, or because too much of the resulting organic material is remineralized in stagnant oxygen minimum zones.

[14] 3. The time required for surface waters to reach intensely hypoxic regions being too long.

[15] Figure 2a and 2b examine the relationship between diffusion coefficient, the sink of oxygen and the equilibrium oxygen saturation within isosurfaces of 20 μM (Figure 2a) and 10 μM (Figure 2b). All else being equal, one would expect the largest hypoxic volumes to lie in the lower right of the figure, with high consumption and low equilibrium saturation. This is not the case, because changing A_{redi} changes the vertical position of hypoxic waters (moving them into shallower, warmer waters).

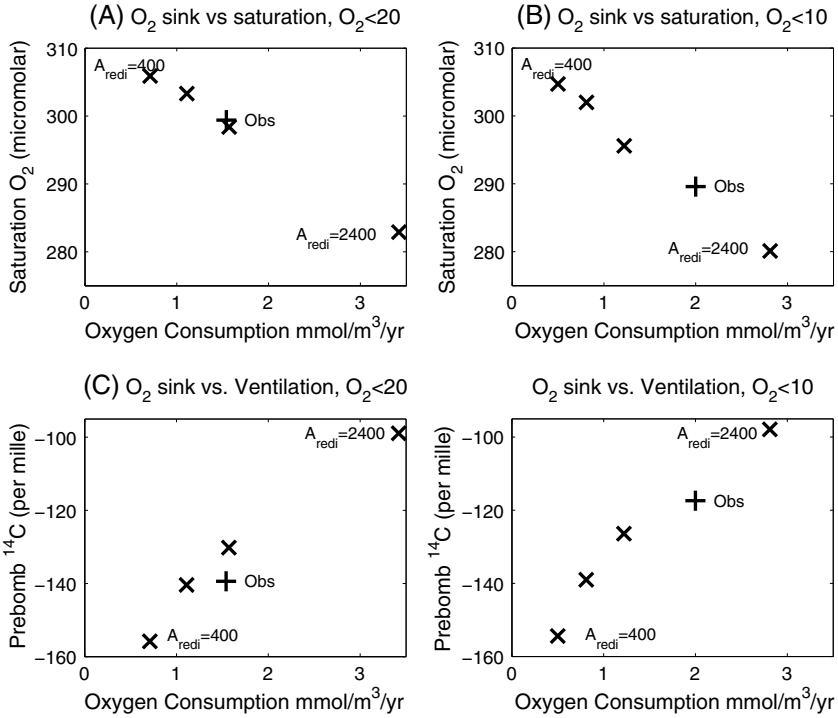

Figure 2. Estimates of the equilibrium oxygen (a and b) saturation, oxygen consumption, and (a and d) ventilation within volumes enclosed by observed isosurfaces of oxygen. plus marks show observations, crosses show the results from the four versions of the ESM2Mc model. Vertical axis shows (top row) equilibrium oxygen saturation and (bottom row) prebomb radiocarbon [*Key et al*., 2004]. Horizontal axis shows oxygen consumption rate in mmol/m^3/yr from *Bianchi et al*. [2012].

[16] Plotting the prebomb radiocarbon [*Key et al*., 2004], which decays as waters move away from the surface outcrop versus the oxygen consumption (Figures 2c, 2d), shows that as mixing coefficient increases, radiocarbon within oxygen isosurfaces also goes up as the bulk of hypoxic waters are found closer to the surface. Matching the observations to the intermodel relationships yields estimates of lateral diffusion coefficient of order 1000–1500 m^2/s for all four plots. There is some sense that the lower values of oxygen are associated with higher diffusion coefficients.

3.2. Satellite-Based Estimate

[17] Figure 3 shows the results of estimating A_{redi} using the satellite-based rate of oxygen demand as a function of oxygen threshold and diapycnal diffusion coefficient. If $K_{\mathrm{v}} = 1 \times 10^{-5}$ m^2/s, the value used in the ESM2Mc model suite and consistent with observations, vertical diffusion is only capable of supplying about 10% of this demand. In order to supply the remainder through lateral diffusion, a diffusion coefficient between 900–1050 m^2/s is required. The result is relatively robust to the oxygen threshold used across an order of magnitude (Figure 3), despite the fact that these different thresholds correspond to different ranges of latitudes and longitudes. For obvious reasons, higher vertical diffusion coefficients allow more supply in the vertical and allow for lower lateral diffusion coefficients.

[18] If the lateral diffusion coefficient is too small to supply sufficient oxygen over the observed volume of suboxic water, then the lateral area of intense suboxia must expand in the horizontal or the vertical. Horizontal expansion allows for a larger aperture for water to be fluxed vertically into suboxic water. Vertical expansion allows for the suboxic zone either to take advantage of higher vertical diffusion coefficients in the deep ocean and near the mixed layer or to open a large aperture for lateral diffusion to bring in oxygen along a greater range of isopycnals. However, because a larger suboxic volume may actually capture more remineralization, the dependence of suboxic volume on diffusion may not be straightforward.

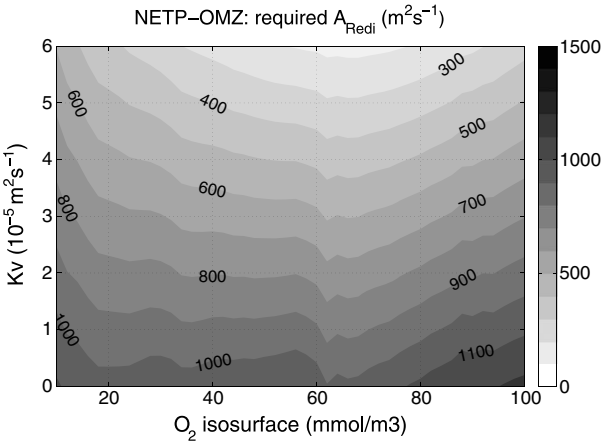

Figure 3. Inferred lateral diffusion coefficient taken from solving equation (3) with both oxygen distributions and satellite-based oxygen consumption rates taken from *Bianchi et al*. [2012]. Vertical axis shows impact of using different vertical diffusion coefficients.

4. Discussion and Conclusions

[19] The satellite-based analysis, radiocarbon distribution and the corresponding results from the model suite are consistent with relatively high lateral diffusive coefficients of around 1000 m^2/s at depths of 200–800 m in the tropics. We acknowledge that both estimates are uncertain. Satellite-based estimates of primary productivity and particle export are subject to considerable uncertainty (with the three products averaged here ranging over a factor of 2 at individual latitudes). Moreover, uncertainties in the remineralization pattern remain, especially within hypoxic waters where there are few measurements. The GFDL models, for example, suppress remineralization within hypoxic waters much more than the satellite-based estimates. Nonetheless, the fact that matching the observed radiocarbon concentrations (which do not depend to first order on biological cycling) requires A_{redi} ~1000 m^2/s suggests that getting the age of low oxygen waters right strongly constrains the integrated consumption of oxygen in such waters. Finally, the results depend on the vertical diffusion coefficient K_v [*Duteil and Oschlies*, 2011]. A much smaller K_v (e.g., as in HadGEM which has $K_v < 3 \times 10^{-6}$ over the top few hundred meters). would likely result in much lower, though possibly unrealistic, productivity (HadGEM2 has a primary productivity of 35 Gt °C/yr versus 59–65 Gt °C/yr in our suite) and thus require a lower lateral diffusion coefficient.

[20] Our results highlight the importance of understanding the processes that ventilate the oxygen minimum zones. One possibility is that small-scale, stationary jets [*Maximenko et al*., 2008] corrugate the edge of the OMZ and thus increase the effective area for lateral diffusion. Another is that the diffusion coefficient is much larger in the east-west direction, as movement in the north-south direction is constrained by angular momentum. Additionally, insofar as oxygen experiences a different pattern of sources and sinks within the ocean interior than do temperature and salinity, the correlation between oxygen and eddy velocity may give rise to a different effective diffusion coefficient. Finally, the eddies that are most important for mixing on these small scales may have a more complex vertical structure that is weakly expressed in altimetric measurements.

[21] **Acknowledgments.** Support under NSF grant EAR-1135382 and DOE grant DE-SC0007066 is gratefully acknowledged. Daniele Bianchi was supported by the Canadian Institute for Advanced Research (CIFAR) Earth System Evolution Program.

[22] The Editor thanks one anonymous reviewer for his/her assistance in evaluating this paper.

References

Behrenfeld, M. J., and P. G. Falkowski (1997), Photosynthetic rates derived from satellite-based chlorophyll concentration, *Limnol. Oceanogr.*, *42*, 1–20.

Bianchi, D., J. P. Dunne, J. L. Sarmiento, and E. D. Galbraith (2012), Data-based estimates of suboxia, denitrification and N_2O production in the ocean and their sensitivities to dissolved O_2, *Global Biogeochem. Cycles*, *26*, GB2009, doi:10.1029/2011GB004209.

Carr, M.-E. (2002), Estimation of potential productivity in Eastern Boundary Currents using remote sensing, *Deep Sea Res. Part II*, *49*, 59–80.

Dunne, J. P., R. A. Armstrong, A. Gnanadesikan, and J. L. Sarmiento (2005), Empirical and mechanistic models of particle export, *Global Biogeochem. Cycles 19*, GB4026, doi:10.1029/2004GB002390.

Dunne, J. P., J. L. Sarmiento, and A. Gnanadesikan (2007), A synthesis of global particle export from the surface ocean and cycling through the ocean interior and on the sea floor, *Global Biogeochem. Cycles*, *21*, GB4006, doi:10.1029/2006GB002907.

Dunne, J. P., A. Gnanadesikan, J. L. Sarmiento, and R. D. Slater (2010), Technical description of the prototype version (v0) of Tracers of Phytoplankton with Allometric Zooplankton (TOPAZ) ocean biogeochemical model as used in the Princeton IFMIP model, *Biogeosciences*, *7*, 3593, Suppl. http://www.biogeosciences.net/7/3593/2010/bg-7-3593-2010-supplement.pdf.

Duteil, O., and A. Oschlies (2011), Sensitivity of simulated extent and future evolution of marine suboxia to mixing intensity, *Geophys. Res. Lett.*, *38*, L06607, doi:10.1029/2011GL046877.

Galbraith, E. D., A. Gnanadesikan, J. P. Dunne, and M. R. Hiscock (2010), Regional impacts of iron-light colimitation in a biogeochemical model, *Biogeosciences*, *7*, 1043–1064.

Galbraith, E. D., et al. (2011), The impact of climate variability on the distribution of radiocarbon in CM2Mc—A new earth system model, *J. Clim.*, *24*, 4230–4254.

Gnanadesikan, A., J. P. Dunne, and J. John (2012), Understanding why the volume of suboxic waters does not increase under centuries of global warming in an Earth System Model, *Biogeosciences*, *9*, 1159–1172.

Gruber, N., and J. L. Sarmiento (1997), Global patterns of marine nitrogen fixation and denitrification, *Global Biogeochem. Cycles*, *11*, 235–266, doi:10.1029/97GB00077.

Hartnett, H., and A. Devol (2003), Role of a strong oxygen-deficient zone in the preservation and degradation of organic matter: A carbon budget for the continental margins of northwest Mexico and Washington State, *Geochim. Cosmochim. Acta*, *67*, 247–264, doi:10.1016/S0016-7037(02)01076-1.

Jones, C. D., et al. (2010), The HadGEM2-ES implementation of CMIP5 centennial simulations, *Geosci. Mod. Dev.*, *4*, 543–570.

Jungclaus, J. H., et al. (2010), Climate and carbon-cycle variability over the last millennium, *Clim. Past*, *6*, 723–727.

Key, R. M., A. Kozyr, C. L. Sabine, K. Lee, R. Wanninkhof, J. L. Bullister, R. A. Feely, F. J. Millero, C. Mordy, and T.-H. Peng (2004), A global ocean carbon climatology: Results from the Global Data Analysis Project (GLODAP), *Global Biogeochem. Cycles*, *18*, GB4031, doi:10.1029/2004GB002247.

Ledwell, J. R., A. J. Watson, and C. S. Law (1998), Mixing of a tracer in the pycnocline, *J. Geophys. Res.*, *103*, 21,499–21,529.

Marra, J., C. Ho, and C. Trees (2003), An alternative algorithm for the calculation of primary productivity from remote sensing data, *Tech. Rep. LDEO-2003-1*, Lamont-Doherty Earth Observatory, Palisades, N. Y.

Maximenko, N. A., O. V. Melnichenko, P. P. Niiler, and H. Sasaki (2008), Stationary mesoscale jet-like features in the ocean, *Geophys. Res. Lett.*, *35*, L08603, doi:10.1029/2008GL033267.

Ollitraut, M., and A. Colin de Verdiere (2002), SOFAR floats reveal midlatitude intermediate North Atlantic General Circulation. Part I A Lagrangian descriptive view, *J. Phys. Oceanogr.*, *32*, 2020–2033.

Redi, M. H. (1982), Ocean isopycnal mixing by coordinate rotation, *J. Phys. Oceanogr.*, *12*, 1154–1158.

Seferian, R. M., L. Bopp, M. Gehlen, J. C. Orr, C. Ethe, P. Cadule, O. Aumont, D. Salas y Melia, A. Voldoire, and G. Madec (2012), Skill assessment of three earth system models with common marine biogeochemistry, *Clim. Dyn.*, *40*, 2549–2573, doi:10.1007/s00382-012-1362-8.

Stramma, L., S. Schmidtko, L. A. Levin, and G. C. Johnson (2010), Ocean oxygen minima expansions and their biological impacts, *Deep Sea Res. Part I*, *57*, 587–595.

Visbeck, M., J. Marshall, T. Haine, and M. Spall (1997), Specification of eddy transfer coefficients in coarse-resolution ocean models, *J. Phys. Oceanogr.*, *27*, 381–402.